Aggregation-Induced Emission Hot Paper

How to cite: *Angew. Chem. Int. Ed.* **2022,** *61,* e202116834
International Edition: doi.org/10.1002/anie.202116834
German Edition: doi.org/10.1002/ange.202116834

Transforming Dyes into Fluorophores: Exciton-Induced Emission with Chain-like Oligo-BODIPY Superstructures

Lukas J. Patalag, Joscha Hoche, Roland Mitric, Daniel B. Werz, and Ben L. Feringa**

Abstract: Herein we present a systematic study demonstrating to which extent exciton formation can amplify fluorescence based on a series of ethylene-bridged oligo-BODIPYs. A set of non- and weakly fluorescent BODIPY motifs was selected and transformed into discrete, chain-like oligomers by linkage via a flexible ethylene tether. The prepared superstructures constitute excitonically active entities with non-conjugated, Coulomb-coupled oscillators. The non-radiative deactivation channels of Internal Conversion (IC), also combined with an upstream reductive Photoelectron Transfer (rPET) and Intersystem Crossing (ISC) were addressed at the monomeric state and the evolution of fluorescence and (non-)radiative decay rates studied along the oligomeric series. We demonstrate that a "masked" fluorescence can be fully reactivated irrespective of the imposed conformational rigidity. This work challenges the paradigm that a collective fluorescence enhancement is limited to sterically induced motional restrictions.

Introduction

In the mid 1930s Jelley and Scheibe independently discovered the influence of dye aggregation on the spectral response and described a phenomenon that was later termed J-aggregation.[1,2] A red-shifted, usually strongly amplified absorption, often accompanied by narrowed bandwidths,[3] was recognized as the distinctive spectral signature. Photophysically it originates from a collective or coherent excitation event of an ensemble of π-chromophores, which evokes either a red-shifted excitation energy (J-type coupling) as observed by its discoverers or an analogous blue-shifted absorption band (H-type coupling) depending on the geometrical parameters of the aggregation.[4–8] After Davydov[9] and Frenkel[10,11] introduced quantum-mechanical descriptions of the process scientific progress finally disclosed that defined dye aggregation with resulting exciton formation is not just an artificial lab curiosity but widely abundant in nature's unique strategy to harvest light and transform photon energy into charge gradients as exploited by the photosynthetic apparatus.[12–14] Although the photophysical outcome of an aggregation can be concertedly modulated,[15,16] it remains a challenging, multicausal process. Increasing effort is therefore invested to enable J-aggregation also within an intramolecularly constrained conformational space.[17–19] To this end various dye scaffolds were linked in a J-type fashion directly at their core moiety (sp^2–sp^2)[20–24] or via alkynyl tethers[25–30] to furnish homo- and hetero-oligomeric superchromophores[31] with characteristic properties, such as exceptionally high extinction coefficients, narrowed absorption[18] and/or emission[27] bandwidths, solvent-dependent intramolecular excitation energy transfers (EET),[32] but also an enhanced quantum yield of fluorescence.[24,25,28,31,33] Although this effect might appear to contradict Englman and Jortner's *energy gap law*[34] it can be in fact rationalized by combining the latter with Kasha's exciton theory.[35–37] However, photoinduced distortive relaxations and intramolecular charge transfer processes can easily overrule a radiative decay of a J-aggregate resulting in decreased emissions[23,29,30,38–41] or even a complete loss of fluorescence at the oligomerized state.[42,43] For instance, while Lambert et al. reported an amplified fluorescence with a squaraine-homodimer from $\Phi_F = 0.62$ to 0.80,[28] J-type arranged BODIPY polymers (linked via the β-position) show lower emission intensities.[20,30,38,39] In most of the studies a fluorescence property has been improved based on intermolecular or superstructural rigidifications[44] either with an already strong emitter and/or with rather low amplifications,[18,28,33] while correlations to excited state dynamics have often not been investigated or remained elusive. As an extension to our previous investigation on strongly fluorescent BODIPY monomers that we integrated into ethylene-bridged superchromophores,[18] we now expound how non- or weakly fluorescent species ($\Phi_F \approx 0.05$)

[*] Dr. L. J. Patalag, Prof. Dr. B. L. Feringa
University of Groningen,
Stratingh Institute for Chemistry,
Nijenborgh 4, 9747 AG, Groningen (The Netherlands)
E-mail: y0067041@gmail.com
b.l.feringa@rug.nl

J. Hoche, Prof. Dr. R. Mitric
Universität Würzburg,
Institute of Physical and Theoretical Chemistry,
Am Hubland, 97074 Würzburg (Germany)

Prof. Dr. D. B. Werz
Technische Universität Braunschweig,
Institute of Organic Chemistry,
Hagenring 30, 38106 Braunschweig (Germany)

that forfeit their emission due to an IC-, ISC- or a preceding rPET-process are able to fully regain their fluorescence property ($\Phi_F \approx 0.90$) when linked by the same ethylene spacer unit. This intramolecular linkage widely preserves the autonomy of the integrated π-systems and conceptually resembles an intermolecular approach based on the conformational instability and the missing π-conjugation.[20-33] For this purpose, we have transformed a set of tailor-made BODIPY monomers into a series of oligo-BODIPYs and investigated the photophysical outcome by optical spectroscopy and computations. Figure 1 presents an overview of the BODIPY species studied in this work and relates the structures to the corresponding prevailing non-radiative decay processes.

Theoretical Background

The quantum yield of fluorescence Φ_F can be generally expressed as an interplay of excited state decay rates via Equation (1):

$$\Phi_F = \frac{k_r}{k_r + k_{nr}} = \frac{k_r}{k_r + k_{IC} + k_{ISC}} \quad (1)$$

High values of Φ_F can be either achieved by increasing the radiative decay rate k_r, by mitigation of its non-radiative counterpart k_{nr} or, most efficiently, by influencing both rates in a beneficial direction. The non-radiative decay process can furthermore be expanded according to the involved multiplicity giving k_{IC} for a transfer in between states of equal multiplicity (Internal Conversion or IC) and k_{ISC} in case of different multiplicities (Intersystem Crossing or ISC). Prior to these decay pathways, however, molecular moieties can also induce a charge separation and form charge-transfer states that are typically dark. If the excited π-system (dye unit) accepts an electron this process is called reductive photoelectron transfer (rPET).

In an excitonically active J-aggregate[46] all these terms can undergo significant variations. First, for the radiative decay process, it has been theoretically predicted that the radiative decay rate $k_{r,N}$ increases proportionally with number of integrated dye units N:[47]

$$k_{r,N} \approx |\mu_{eg,N}|^2 \left(\frac{4n}{3c^3}\Delta E^3\right) \approx N|\mu_{eg,1}|^2 \left(\frac{4n}{3c^3}\Delta E^3\right) \approx N k_{r,1} \quad (2)$$

ΔE and n denote the energy gap/emission energy and the refractive index of the medium, respectively. Owing to the relatively small red-shift of a J-aggregate ΔE_N and ΔE_1 can be approximated with $\Delta E = \Delta E_N \approx \Delta E_1$. The resulting linear dependency between $k_{r,N}$ and $k_{r,1}$ then originates in an amplified electronic coupling between ground and excited state, which is determined by the transition dipole moment μ_{eg}. For a bright state of a J-aggregate with N units it follows, that the squared transition dipole moment of the J-aggregate $|\mu_{eg,N}|^2$ is a sum of the squared transition dipole moments of the single interacting units $|\mu_{eg,N}|^2 = N|\mu_{eg,1}|^2$. The uniform de-excitation then results in a superradiant emission[48] with decreased fluorescence lifetimes.

For delocalized excitons,[49] the scaling of the non-radiative decay rate k_{IC} with the number of coupled dye

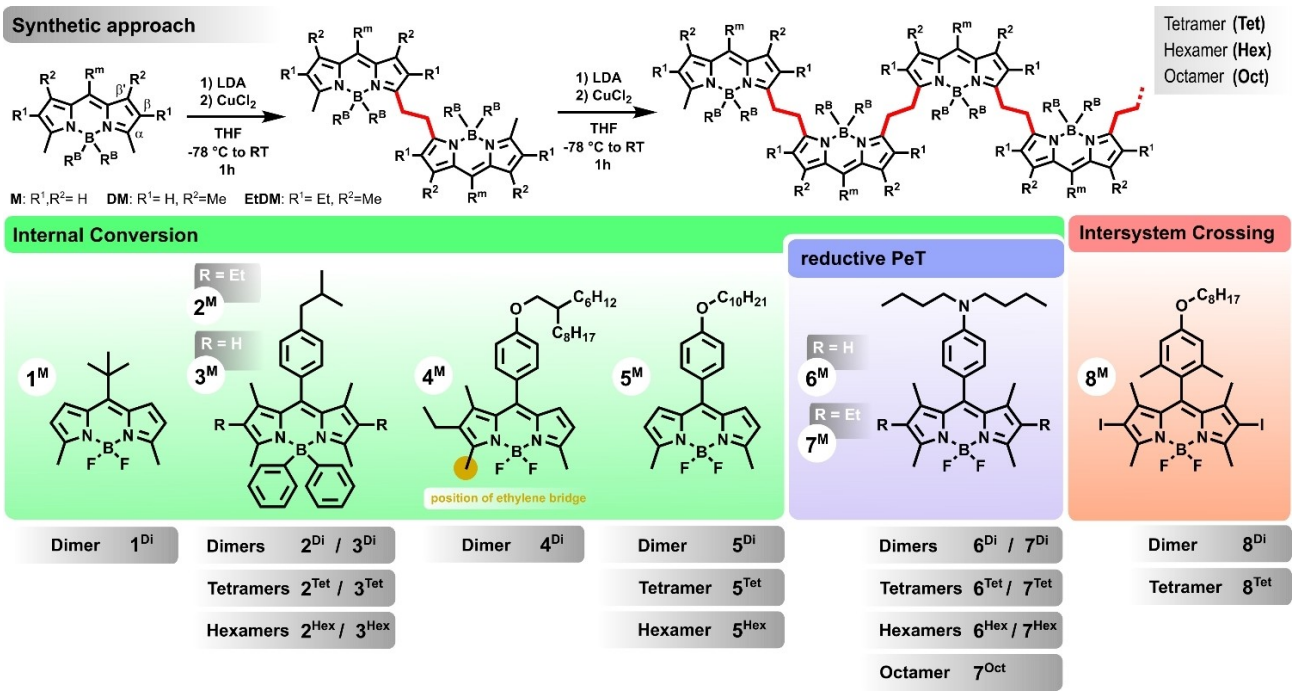

Figure 1. Synthetic scheme with the engaged pyrrole substitution patterns M, DM and EtDM and obtained compound range with assignment of synthesized BODIPY monomers to corresponding deactivation pathways responsible for the suppressed emission at the monomeric state. The Internal Conversion (IC) section encompasses also the rPET mechanism which happens prior to the decay to S_0.

units can also be derived.[47,50] In the case of weakly displaced potential energy surfaces, where the harmonic approximation is valid, the most common approach to estimate the internal conversion rate is based on the *energy gap law* (EGL) by Englman and Jortner.[34] We will adopt the notation of the EGL from ref. [47] that reads:

$$k_{IC}^{EGL} \approx \frac{u_{IC}}{2\sqrt{2\pi}} C^2 e^{-S\cdot d} \sqrt{\frac{1}{x}} \exp\left(-x\left[\log\left(\frac{x}{S\cdot d}\right)-1\right]\right) \quad (3)$$

The normal mode frequencies and Huang–Rhys factors are replaced by the number of effective promoting modes d that carry an average Huang–Rhys factor S. The length of the non-adiabatic coupling vector between the initial and final state is denoted as C. If all quantities are given in atomic units, the factor $u_{IC} = 4.134 \times 10^{16}\ s^{-1}$ converts the rate to s^{-1}. The quantity $x = \Delta E/\hbar\omega_{eff}$ is the number of quanta in the effective modes that is required to match the energy gap between the electronic states. Some of us have recently derived the following scaling relations.[47] The number of promoting modes scales linearly with the number of monomers $d_N = Nd_1$. Using the second Hellmann-Feynman theorem it follows that the length of the non-adiabatic coupling vector stays approximately constant ($C_N \approx C_1$) and the Huang–Rhys factors follow a scaling with N^{-2}. In addition, some further approximations can be introduced: If the influence of the excitonic coupling on the electronic energy gap is small, then $\Delta E_N \approx \Delta E_1$ and $x_N \approx x_1$ stay approximately constant. Furthermore, the scaling relations strongly dominate the number of quanta to match the energy gap so that their impact on the prefactor ($\exp(-Sd)$) is negligible. Using these approximations we get the following scaling of the internal conversion rate:

$$k_{IC,N}^{EGL} \approx \left(\frac{1}{N}\right)^x k_{IC,1} \quad (4)$$

However, we observed that the scaling of the Huang–Rhys factor is only valid in the limit of large oligomers/polymers. In rather small aggregates, such as the ones studied in this work, the displacement of the promoting modes stays approximately constant or decreases only slightly with the number of monomers.[47] As a result, the exponent might be much smaller than x for the comparison of monomers ($N=1$) to aggregates with $N \leq 8$. Thus, an inverse linear scaling might be considered as an upper bound for the internal conversion rate that is mediated by vibronic coupling:

$$k_{IC,N}^{EGL} \lesssim \frac{1}{N} k_{IC,1} \quad (5)$$

It can be seen that in growing aggregates, for which the harmonic approximation is valid (e.g. no presence of conical intersections), a strong reduction of the non-radiative decay rate k_{IC} should be observed. Together with the amplification of k_r according to Equation (1) J-aggregates have the potential to develop strong emissions even in the near-infrared region[51] despite their typically red-shifted main absorptions. In the following, we will present experimental data for the decay rates k_r and k_{nr} as functions of N.

Results and Discussion

Synthesis and Conformational Analysis

BODIPY scaffolds[52–61] bearing an α-methyl group are suitable substrates for an oxidative coupling strategy to furnish a series of ethylene-bridged oligomers in a straightforward two-step approach (see Figure 1, top), a general method that is applicable to various building blocks.[62,63] While the first step leads to dimeric species exclusively with yields up to 75 %, a subsequent oligomerization gives a range of n(dimeric) oligomers ($n = 1, 2, 3, 4$).[18] Owing to the transition dipole moment of S_1 that is oriented along the long axis of the BODIPY motif the linkage results in a geometrical predisposition for J-type coupling. Since a conformational exchange at the ethylene bridge occurs in the picosecond regime standard NMR spectroscopy is ill-suited to detect possible conformational distributions. We thus decided for a computational approach. First, we envisaged finding ground-state global minimum geometries of simple dimeric structures assuming that resulting lowest energy geometries should then be transferable to higher homologs with reasonable accuracy. Owing to the large structural diversity of our compound range we decided for a representative dimeric BODIPY prototype with a *meso* substituent R^m = Phenyl as an adequate, geometrical approximation to account for most series in Figure 1 (for series **2** and **3** with phenyl-equipped boron centers an additional study with similar results is presented in the Supporting Information). We furthermore modified the dipyrrin substitution pattern according to our set of compounds: 2-methyl (M) in the series **1**, **5** and **4**; 2,4-dimethyl (DM) in series **3** and **6** and finally 3-ethyl-2,4-dimethyl (EtDM) as present in the series **2**, **4** and **7**. After an initial conformational analysis with a force-field-based Monte Carlo sampling resulting dominant geometries were furthermore optimized at the DFT-level and refined with a final single-point calculation using a robust double-hybrid functional (DSD-BLYP/TZVPP) with D3 dispersion correction.[64] Figure 2 depicts the conformational space at the ethylene bridge and contrasts dominant microstructures with free Gibbs energies to outline an estimated ranking. While the energetic discrimination in EtDM-derived series is highest as a result of the steric repulsion of β-ethyl residues that favor the *saddle2* arrangement, dimers with M and DM dipyrrin cores exhibit a wider conformational space and might adopt *staggered*, *saddle* and even the gauche conformation *SC-cis* with similar preference. A nearly equivalent ranking has been found by some of us in ref. [18]. Thus, we conclude with some caution that *saddle2* in case of the EtDM-derived series and a potential coexistence of various geometries for M- and DM-derived congeners are the structural equivalents in accordance with the obtained spectroscopic results below, also for higher homologs with multiple ethylene bridges.

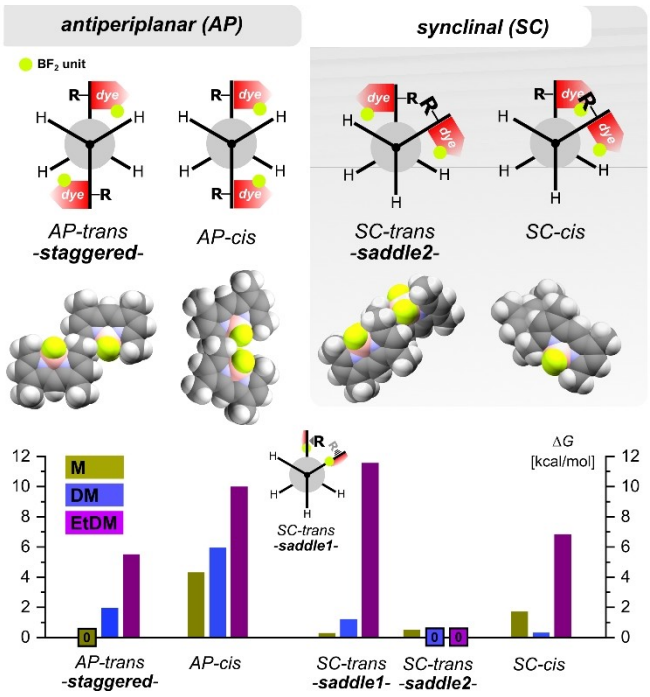

Figure 2. Conformational space of the ethylene bridge (Newman projections) with microstructures of a representative dimer platform (*meso* substituent: $R^m = Ph$). Computationally derived relative free Gibbs energies as a function of M-, DM- and EtDM derived dipyrrin core structures, respectively. Depicted microstructures refer to the DM case exemplarily ($R^m = Ph$ is replaced by $R^m = H$ for better visualization.)

Spectroscopy

Steady-state absorption and emission spectra, which we recorded in DCM, THF and toluene, support the conformational selection of our computational study. All oligo-BODIPY series develop a consistent increase of extinction coefficients with growing chain-lengths accompanied by a strong red-shift of absorption and emission independent of solvent polarity, which supports the global linear morphology arranged by the ethylene tether. To exclude contributions of intermolecular aggregation effects, all spectra were additionally recorded at different dilutions without observing changes in the spectral characteristics in all cases. The range distribution of spectrally derived excitonic coupling constants V is quite homogeneous (ca. $-600\,cm^{-1}$ to $-800\,cm^{-1}$) indicating prevailing J-type coupling conditions for all series. A pronounced excitonic splitting[65,40] which would arise from bright H-type coupling contributions specifically at geometries that enforce a deviation from the global structural linearity (*AP-cis* and *SC-cis*) was not observed explicitly in shape of distinct high-energy peaks but contributes to the tailing of the absorption bands especially in case of the M- and DM-derived series with unshielded ethylene linkers and conformational instabilities. Figure 3 illustrates the spectral evolution of two series with different BODIPY substitution patterns and deactivation channels (series **3** and series **7**). Both examples are depicted as two extreme cases of the compound range presented (for more spectra see Supporting Information, chap. 4.1). In case of series **3** absorption and emission widely appear as mirror images, corresponding bands however are broad and seem to be an overlay of at least two distinct absorption events, especially for $\mathbf{3}^{Di}$. This might indicate an excitonically intensified vibronic progression, the aforementioned coexistence of virtually isoenergetic geometries or the interplay of both. Such complex spectra were observed for many compounds of this study affecting also emission profiles (see series $\mathbf{3}/\mathbf{3}^{Di}$ and $\mathbf{5}/\mathbf{5}^{Di}$, Supporting Information). This is different for series **7**, where β-ethyl groups (EtDM core) impose additional steric restrictions and enable a fixation of adjacent BODIPY units in the *saddle2* conformation. The exciton delocalization thus becomes spectroscopically evident and is manifested in narrowed absorption and emission bandshapes, which are compressed (fwhm) from $850/880\,cm^{-1}$ ($\mathbf{7}^{M}$) to $270\,cm^{-1}$ ($\mathbf{7}^{Oct}$), corresponding to an effective coherence length of:

$$N_{eff} \approx 10 \text{ according to } \sqrt{N_{eff}} = \frac{\Delta\tilde{\nu}^{\text{monomer}}_{2/3}}{\Delta\tilde{\nu}^{\text{oligomer}}_{2/3}}$$

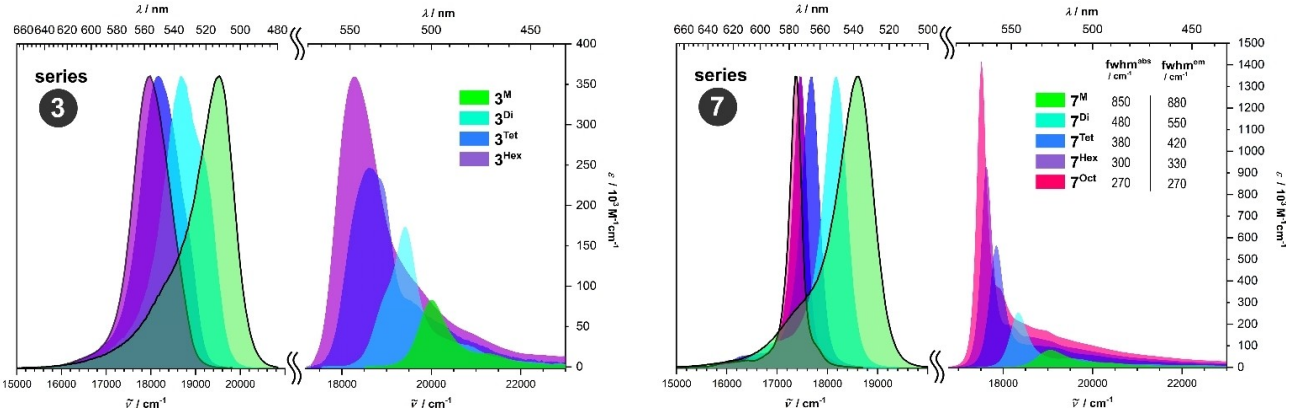

Figure 3. Series **3** and series **7** with absorption spectra (right) and emission spectra (left), respectively, in toluene at room temperature (RT). Emission is normalized. For series **7** full width at half maximum values (fwhm) are given for main absorption and emission bands.

where $\Delta\tilde{\nu}$ represents the linewidth at two-thirds of the maximum height of the corresponding main absorption band.[66] This result is in reasonable agreement with the number of dye units in the octamer and verifies a strongly delocalized exciton in series **7**.

We next examined the impact of the oligomerization on radiative decay rates k_r as well as quantum yields of fluorescence Φ_F and rationalized a correlation with the deactivation channel involved. Except for series **8** (all solvents) and series **6** (DCM, THF) k_r trends widely proportionally with the number of integrated dye units N (Figure 4A) as predicted by theory for strongly coupled dye aggregates [see Eq. (2)]. An exception is made for series **6** and **7** (rPET channel) where k_r increases disproportionally (**6**^{M} to **6**^{Di}, 10-fold; **7**^{Di} to **7**^{Tet}, 5-fold, see normalized plot). The tendency for a weak flattening of the curves at higher homologs might indicate the statistical increase of conformational disorder with higher contributions of heterogeneous coupling conditions or might be traced back to the decreasing emission energy ΔE_N, which was ignored in the approximation of Equation (2). Non-radiative rates k_{nr} show a more disparate evolution along the series (Figure 4B). A consistent decrease is only present in series **2** and **3** and cannot be specified for series **1** and **4** owing to the short oligomeric compound range in these cases. Despite this variety of excited state scenarios the quantum yield of fluorescence Φ_F (Figure 4C) increases strongly upon oligomerization in all series, except for the ISC case. In series **1**, **2**, **3** and **5** (IC decay mechanism) as well as in series **6** and **7** (toluene) the fluorescence is virtually maximized at the highest homolog. The absorption and emission spectra for most series (except series **4** and **7**) show no clear band narrowing, although the radiative rates detected prove high delocalization lengths. However, this can be explained by the specific conformational stability within the BODIPY series (see Figure 5). As demonstrated by the energetic ranking in Figure 2, the rigidification of the ethylene linker units by β-ethyl groups (EtDM core) and the exclusive *saddle2* microstructure in this case leads to consistently defined superstructures at higher homologs disclosing the well-known exchange narrowing effect.

In cases where the ethylene bridge is less shielded (series **1**, **3**, **5**, **6** and **8**) or distorted by remote interactions (BPh_2 groups in series **2** and **3**) the presence of multiple microstructures within one superstructure leads to strongly differing excitonic couplings (off-diagonal disorder) and a redistribution of oscillator strengths within the exciton manifold.[67] Based on this micostructural diversity a manifold of co-existing superstructures emerges in addition. In order to address this effect we have simulated absorption spectra and excitonic couplings V of all representative dimer microstructures (see Figure 2) at the TDDFT level (see Table S3) and used Boltzmann populations (see donut charts in Figure 5, Figure S149) for simulation of absorption spectra (outlined graphs in Figure 5, Figure S150). Assuming that the H-type arrangement *AP-cis* is thermally inaccessible for M-, DM- and EtDM-derived series, V values are negative, yet quite homogeneous for *AP-trans*, *saddle1* and *saddle2* (−600 to −1000 cm^{-1}) but positive in case of the H-type microstructure *SC-cis* (800–1600 cm^{-1}). Since a *SC-cis* contribution thus results in higher excitonic couplings(up to 1600 cm^{-1}) the degree of exciton delocalization according to $\left|\frac{V}{\Delta E_{AB}}\right|$ is unaffected by the sign of V and even tolerates a higher site energy disorder ΔE_{AB}. These heterogeneous coupling contributions within one superstructure clearly show that a superstructure manifold will lead to a superposition of individual absorption spectra that effectively hide the exchange narrowing effect. Analogous to the

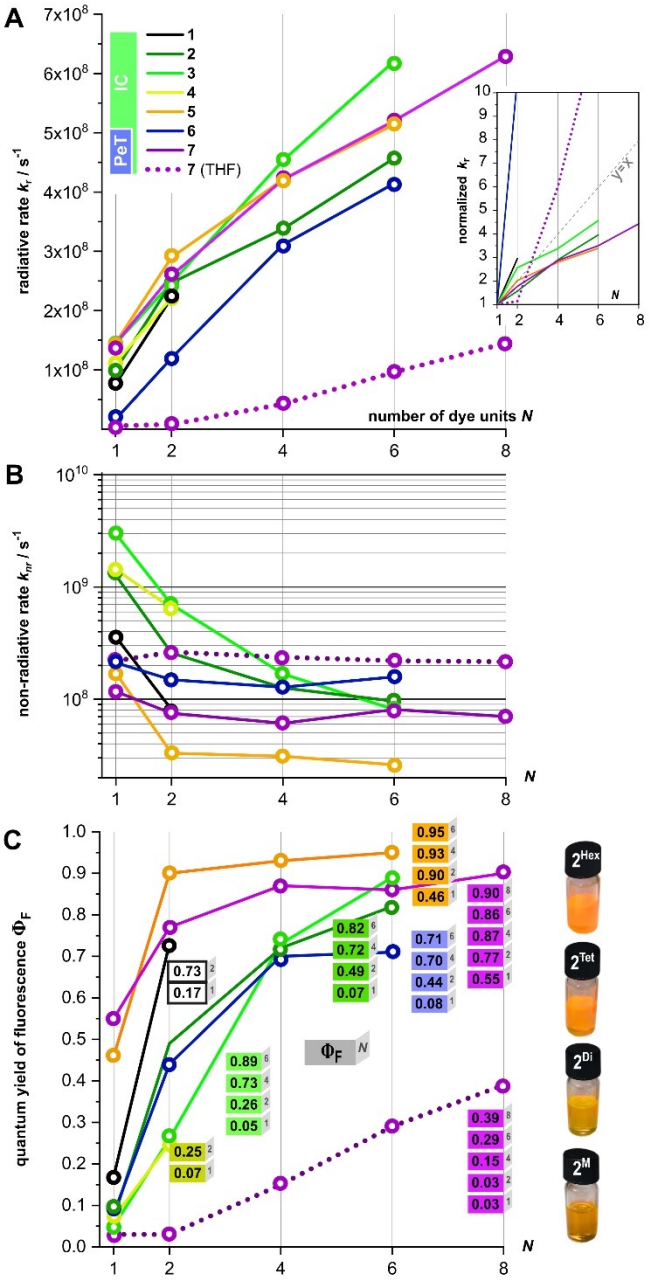

Figure 4. A) Evolution of (normalized) radiative decay rates k_r according to $k_r = \Phi_F/\tau_F$. B) Evolution of non-radiative decay rates k_{nr} according to $k_{nr} = (1-\Phi_F)/\tau_F$ in logarithmic scale. C) Quantum yields of fluorescence Φ_F along the growing oligomers in toluene. Φ_F values are given in boxes starting from the monomer at the bottom.

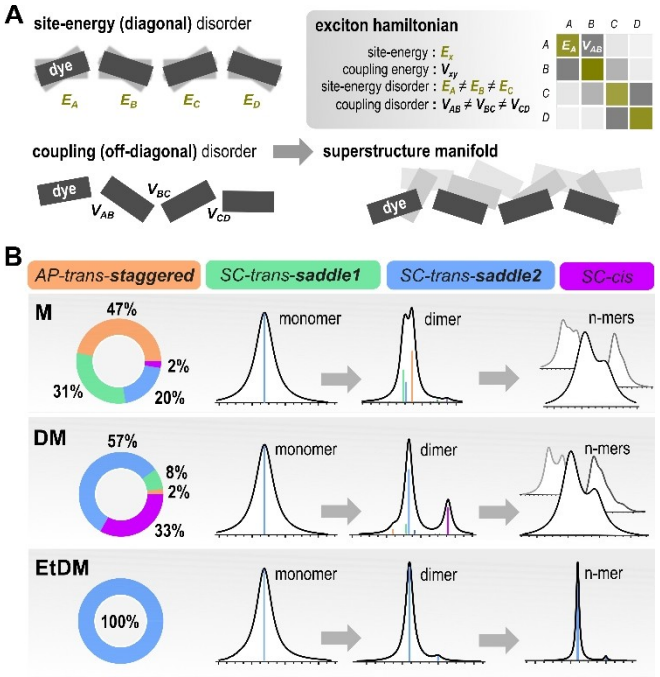

Figure 5. A) Illustrated disorder contributions and B) evolution of dimer (oligomer) bandshapes based on the microstructural compositions (Boltzmann population) derived from Gibbs free energies (representative M-, DM- and EDM-dimer platform / Figure 2).

absorption, the emission originates also in a manifold of co-existing, excited superstructures. The complexity of the absorption profiles is thus partially mirrored on the emission side except for the higher excited states that will mostly equilibrate to S_1 according to Kasha's rule. We found evidence for the co-existence of multiple emissive geometries in complex lifetime compositions of fluorescence decay curves and emission-wavelength-dependent lifetime measurements (see Figures S34, S59). In the following we will discuss each series separately and review the specific decay mechanisms involved.

BODIPY Series 1

BODIPY $\mathbf{1}^{\mathbf{M}}$ bearing a sterically demanding *tert*-butyl group at the *meso* position is weakly fluorescent in DCM, THF and toluene ($\Phi_F \approx 0.16$–0.22). In addition, the emission band appears unusually broad for a BODIPY motif pointing towards a dominant excited state relaxation channel. A similar species without α-methyl groups has been computationally investigated by Jiao and Corminboeuf,[68,69] who found a conical intersection at a puckered dipyrrin geometry with an out-of-plane distorted *tert*-butyl group as the responsible decay channel. We found minimum energy conical intersections (MECI's), which structurally correspond very well to those presented previously.[68] The excited state barrier between the Franck–Condon geometry and the MECI are quite small in the monomer (see Figure 6D) as well as in the dimer (see Figure S151) with values of 0.09 eV

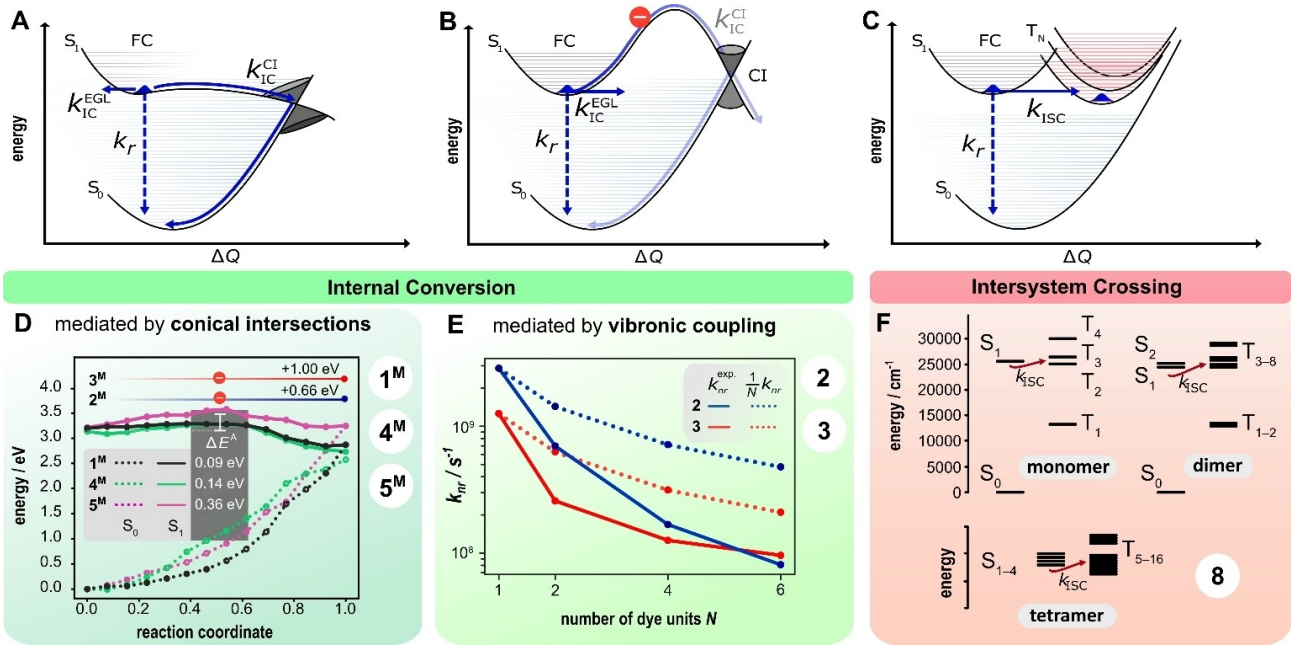

Figure 6. A–C) Energetics and relaxation pathways after excitation into the bright exciton state of a J-aggregate with illustrations of the conical intersection pathway IC^{CI} (A), the vibrationally controlled IC mechanism IC^{vib} (B) and the ISC decay (C). D) Minimum energy pathways between the Franck–Condon minimum and the conical intersection for BODIPY monomers $\mathbf{1}^{\mathbf{M}}$, $\mathbf{4}^{\mathbf{M}}$ and $\mathbf{5}^{\mathbf{M}}$ as well as the inaccessible MECI's of $\mathbf{2}^{\mathbf{M}}$, $\mathbf{3}^{\mathbf{M}}$ for comparison. E) Graphical juxtaposition of experimental, non-radiative decay rates and theoretical counterparts according to the scaling relation derived in Equation (6) for series **2** and **3**. F) Energy diagram of the singlet and triplet states for monomer, dimer and tetramer of series **8**

and 0.16 eV, respectively, clearly indicating a conical intersection as a prevailing relaxation pathway in S_1. The dimer $\mathbf{1}^{\mathbf{Di}}$ shows a strongly amplified emission ($\Phi_F \approx 0.58$–0.73) accompanied by a doubled radiative rate constant k_r in all three solvent systems as predicted by theory [Eq. (2)]. The oligomerization, however, could not be extended further because of a limited solubility. Albeit of complex shape the emission band of $\mathbf{1}^{\mathbf{Di}}$ is narrowed ($fwhm^E \approx 1200$–$1300\ cm^{-1}$) compared to its monomeric precursor $\mathbf{1}^{\mathbf{M}}$ ($fwhm^E \approx 2100$–$2300\ cm^{-1}$), which reflects a mitigated relaxation process as result of a delocalized excitation energy.

BODIPY Series 2 and 3

The non-radiative deactivation in the monomers $\mathbf{2}^{\mathbf{M}}$ (EtDM core) and $\mathbf{3}^{\mathbf{M}}$ (DM core) incorporating a central $B(Ph)_2$ group[19,70] is even more pronounced, which results in a very weak, solvent-independent fluorescence at the monomeric state ($\Phi_F \approx 0.07$ ($\mathbf{2}^{\mathbf{M}}$), $\Phi_F \approx 0.05$ ($\mathbf{3}^{\mathbf{M}}$)). The mechanism for the quenching process has not been revealed yet, but additional high frequency C–H bonds[70-74] of the installed phenyl residues at the boron center as well as photoinduced interactions between the phenyl residues and the *meso* aryl group are likely to play a key role. In contrast to $\mathbf{1}^{\mathbf{M}}$ we found MECI′s for both monomers that are thermally not accessible since they exceed the Franck–Condon minimum by 0.66 ($\mathbf{2}^{\mathbf{M}}$) and 1.00 ($\mathbf{3}^{\mathbf{M}}$) eV (see Figure 6D). The non-radiative relaxation process should thus be dominated by an internal conversion mediated by vibronic coupling and can be understood qualitatively by using Englman & Jortner's *energy gap law*. Using the scaling relations derived in Equation (5) for the upper bound of k_{IC}. Figure 6E illustrates a good correlation with experimentally obtained non-radiative decay rates, which supports the theoretically derived decrease according to $1/N$ as the upper limit.

Upon oligomerization the fluorescence quantum yield is substantially enhanced in both series and in all solvent systems up to $\Phi_F \approx 0.8$–0.9. Comparing the similar fluorescence enhancements in both series (DM and EtDM core) indicates that the effect is less restricted to a rigid alignment of the coupled dye units but tolerates a certain degree of conformational disorder. However, in case of the structurally rigidified series **2** the β-ethyl substituents lead to a continuous narrowing of emission bands ($fwhm^E \approx 1000\ cm^{-1}$ ($\mathbf{2}^{\mathbf{M}}$), $fwhm^E \approx 500\ cm^{-1}$ ($\mathbf{2}^{\mathbf{Hex}}$)), similarly to but not as pronounced as in series **7**.

BODIPY Series 4 and 5

BODIPYs $\mathbf{4}^{\mathbf{M}}$ and $\mathbf{5}^{\mathbf{M}}$ with torsional freedom at their unsaturated *meso* position are known to generally exhibit a diminished fluorescence.[75,76] A structural congener of $\mathbf{5}^{\mathbf{M}}$ (no α-methyl groups, underivatized *meso* phenyl group) has been computationally studied[68] and a torsional motion of its phenyl ring disclosed as a probable relaxation pathway for a conical intersection mechanism ($\Phi_F \approx 0.05$). In fact, BODIPYs with an unrestricted aryl group at the *meso* position can induce non-directional, rotational motions around the *meso* bond,[77–79] a process which was recently implemented in a rotaxane-BODIPY conjugate by Stoddard et al.[80] Hence, we optimized the MECIs and the corresponding minimum energy paths for $\mathbf{4}^{\mathbf{M}}$ and $\mathbf{5}^{\mathbf{M}}$ and obtained low barriers of 0.14 and 0.36 eV, respectively, which underlines a strong contribution of non-radiative relaxation mechanism through a conical intersection (see Figure 6D). While $\mathbf{4}^{\mathbf{M}}$ was only dimerized owing to its unsymmetrical core structure, its emission could be increased up to fourfold ($\mathbf{4}^{\mathbf{Di}}$, $\Phi_F \approx 0.14$–0.25). Starting from a reasonably strong fluorescence at $\mathbf{5}^{\mathbf{M}}$ the oligomerization up to a hexamer leads to Φ_F values that steadily approach unity. Even though Φ_F is thus quickly maximized already at the dimer $\mathbf{5}^{\mathbf{Di}}$ k_r still increases due to consistently lowered superradiant lifetimes (see Figure 4A). In contrast to related BODIPY rotors, whose motional relaxation can be suppressed e.g. by sterics,[80] aggregation[81] or viscosity[80–85] resulting in reactivated emissions, the enhanced fluorescence of series **4** and **5** is not governed by an interchromophoric stacking process or an imposed steric hindrance that is rationalized nowadays in the frames of restricted intramolecular motion (RIM)[86] or restricted access to a conical intersection (RACl).[87] Instead, the weakly predefined spatial proximity of the ethylene tether generates excitons of sufficient delocalization and stability to maximize a masked fluorescence property. For distinction of this mechanism, also within the concepts of aggregation-induced emission (AIE)[88–90] and folding-induced fluorescence enhancement (FIFE)[16a] we thus propose the term exciton-induced emission (EIE) as a qualified expression for such cases.

BODIPY Series 6 and 7

Series **6** and **7** are equipped with an electron-rich aniline *meso* residue that is known to trigger a dark charge-transfer (CT) state as a consequence of a preceding solvent-dependent, rPET process.[91,92] For the DM-derived series **6** only a very weak emission in all three solvents was detected with low-energy CT emission bands in polar DCM and THF. In non-polar toluene this band is blue-shifted and superimposed with the main emission band. We computed particle and hole densities between ground and excited states for $\mathbf{6}^{\mathbf{M}}$ and $\mathbf{7}^{\mathbf{M}}$ (see Figure S152) that unambiguously prove the existence of a charge transfer state for $\mathbf{6}^{\mathbf{M}}$ and $\mathbf{7}^{\mathbf{M}}$, respectively. While the oligomerization has no impact on the emission in DCM and THF regarding series **6**, the fluorescence efficiency is strongly increased from $\Phi_F = 0.05$ ($\mathbf{6}^{\mathbf{M}}$) to $\Phi_F = 0.71$ ($\mathbf{6}^{\mathbf{Hex}}$) in toluene. The β-ethyl substituted congener $\mathbf{7}^{\mathbf{M}}$ shows similar spectroscopic features in DCM and THF as $\mathbf{6}^{\mathbf{M}}$ ($\Phi_F \approx 0.01$–0.03), however, in toluene a reasonably strong fluorescence ($\Phi_F \approx 0.55$) is already present. The lack of a pronounced CT emission band thus questions the impact of a rPET process in case of this non-polar solvent. Differently to series **6**, however, the emission can now also be gradually increased in DCM and THF ($\mathbf{7}^{\mathbf{Oct}}$, $\Phi_F \approx 0.20$–0.39). While the non-radiative rate stays widely constant the radiative rate k_r shows a disproportional step in

both series (see Figure 4A, normalized plot), which reflects the energetic variation of localized donor and acceptor orbitals responsible for the rPET process. We plotted frontier orbital energies of series **6** and **7** up to the tetramer and found a higher energy gap between the aniline- (donor) and the BODIPY-core-centered orbitals (acceptor) in series **7**,[93] which explains the inhibited rPET mechanism (see Figure S153). The higher energy gap can be clearly attributed to the enhanced electron-richness of the ethyl-equipped EtDM core and, associated therewith, an energetically upshifted exciton manifold. Even though the very weak fluorescence of the monomer $\mathbf{7^M}$ in DCM and THF is hard to determine accurately, we assume that the amplification of emission in this case is largest in our study and to the best of our knowledge unprecedented in literature for a CT-defined decay channel.

BODIPY Series 8

Diiodinated BODIPY motifs[94] are widely non-emissive owing to a rapid ISC process populating a low-energy triplet state. The intersystem crossing efficiency of a very similar diiodinated BODIPY dye has been studied very recently by Grusenmeyer et al. and determined in the range of $10^9\ s^{-1}$, which is roughly one magnitude higher than the radiative rate constant obtained and verified by us rationalizing the pronounced loss of emission.[95] Even though the β-iodine residues in series **8** seem to promote an ordered aggregation sphere at the ethylene bridges (see Figure S138) the emission efficiency is hard to determine accurately ($\Phi_F \approx 0.01$–0.04) and not amplified upon oligomerization. In contrast to the IC rate, the ISC rate is expected to increase with the number of monomeric units because the number of triplet acceptor states expand linearly and in addition to the extended singlet exciton manifold upon oligomerization (see Figure 6F and Table S4). According to Fermi's Golden Rule the coupling between singlet and triplet states is thus enhanced leading to a more efficient intersystem crossing process. Albeit not quantifiable, yet present *in the background* the increase of the radiative rate cannot overcompensate this effect that is sometimes described in the literature as aggregation-induced intersystem crossing.[96] However, in contrast to the very long known phenomenon of aggregation-induced emission, this effect is achieved purely by the electronic interaction of the monomers.

Weak coupling limit

After having studied the impact of EIE on several non-radiative deactivation channels we sought for clarifying the role of the ethylene bridge and the proximity and alignment it provides between the dye units. Thus, we prepared two analogs of dimers $\mathbf{3^{Di}}$ and $\mathbf{5^{Di}}$ where the BODIPY motifs are linked at the *meso* position via a flexible alkyl ($\mathbf{9^{mDi}}$) or an alkoxyaryl ($\mathbf{10^{mDi}}$) tether unit (Figure 7). While $\mathbf{9^{mDi}}$ addresses the vibronically mediated internal conversion channel, $\mathbf{10^{mDi}}$ represents the case of the relaxation through a

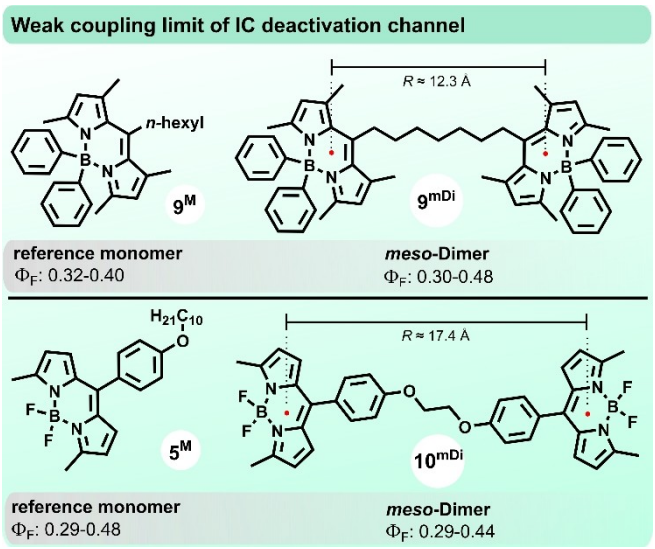

Figure 7. *Meso*-tethered BODIPY dimers as model scaffolds to study the weak coupling limit. Φ_F value range results from different solvent systems. Distance *R* assumes a stretched, all-*anti* conformation. For synthetic details, see Supporting Information.

conical intersection in analogy to $\mathbf{3^{Di}}$ and $\mathbf{5^{Di}}$. Assuming stretched geometries as global minimum structures both dye units are aligned face-to-face in an H-type fashion but are still able to exchange their excitation energy via resonance energy transfer (RET).[97] We performed ground-state semi-empirical molecular dynamic simulations (see Figure S154, S155) to estimate the average interchromophoric distance *R* and obtained values of 10.4 Å ($\mathbf{9^{mDi}}$) and 13.4 Å ($\mathbf{10^{mDi}}$). UV- and emission spectra give no hints for a coexistence of photophysically differing conformers, which underlines a rapid inter-conformational exchange. The distance relations in these dimer structures resemble the ones found for instance in light-harvesting frameworks,[97] MOFs[98–100] and dye-containing nano-structures.[101,102] Comparing now the *meso*-linked dimer $\mathbf{9^{mDi}}$ with its monomeric reference $\mathbf{9^M}$ reveals very similar spectral properties except for the trivial doubling of the extinction coefficient. Radiative decay rates and Φ_F values, however, do not increase for $\mathbf{9^{mDi}}$ and are widely identical with values obtained for $\mathbf{9^M}$ within the instrumental error. An even higher spectral and photophysical accordance was found for the compound pair $\mathbf{5^M}$ and $\mathbf{10^{mDi}}$ with an extended interchromophoric distance and an even smaller excitonic coupling energy indicating the absence of a delocalized exciton. The exchange of excitation energy of a two-level quantum system can be approximated as a coherent oscillation with the frequency $\omega_R = \frac{E_2 - E_1}{\hbar} = \frac{2V}{\hbar}$, also known as Rabi oscillation. Excitonic coupling constants *V* derived either from TDDFT computations or explicitly (see Supporting Information, Table S5) give respective frequencies in the range of ca. 1700–6800 ns^{-1} ($\mathbf{9^{mDi}}$) and 1200–4400 ns^{-1} ($\mathbf{10^{mDi}}$) depending on the level of theory. Assuming a (Homo-)FRET approach[96] and using Equation S5 as another rough approximation gave corresponding rates of 500–800 ns^{-1} for $\mathbf{9^{mDi}}$ and 500–600 ns^{-1} for $\mathbf{10^{mDi}}$. Thus, with the small coupling energies of ca. 20–110 cm^{-1}

both dimeric systems are still able to transfer excitation energy back and forth several hundred times within the fluorescence lifetime of ca. 2–4 ns. However, an evident impact on excited state relaxations and Φ_F values can not be observed. From these results we conclude that such a symmetric and bidirectional RET process is neither sufficient to slowdown a non-radiative decay process related to energy barriers of a conical intersection process, nor for a vibronically mediated internal conversion. Instead, sufficient exciton delocalization based on a close, yet less defined proximity, as provided for example by an ethylene bridge, seems to be key to enable an efficient decoupling of nuclear and photoinduced electronic oscillations and unveil an inherent fluorescence property.

Conclusion

Within a mechanistic concept that we practically term exciton-induced emission (EIE) we presented a systematic study of the molecular parameters necessary to enhance or reactivate a structurally disguised emission capacity with exemplary BODIPY scaffolds. In contrast to previous molecular setups that rely on aggregation processes (AIE), molecular rigidifications and π-conjugational connectivities we could engage a flexible ethylene tether unit to achieve maximum enhancements of fluorescence based on exciton delocalization. A certain amount of conformational instability within the chain structures, as present in M and DM-derived species, does not seem to be detrimental to the amplification effect, suggesting a tolerance to higher (off-)diagonal disorders or even a transient trapping of excitonic energy on single sites. Along this strategy we demonstrated that non-radiative deactivation processes based on an IC mechanism, from the conical intersection limit to vibronically mediated cases, can be fully suppressed. Especially in the case of the very weak emitters with phenyl-substituted boron centers ($\Phi_F \approx 0.04$–0.08) the fluorescence was virtually maximized at the hexameric state ($\Phi_F \approx 0.79$–0.89). To the best of our knowledge, such extreme amplifications based on a widely unconstrained spatial proximity have not yet been reported for discrete fluorescent entities. Within the frame of IC we additionally proved the attenuation of weakly emissive CT states triggered by an upstream rPET process at conformationally more rigidified EtDM-derived oligo-BODIPYs. In this case the fluorescence of a virtually non-emissive aniline-equipped BODIPY monomer $\mathbf{7^M}$ was amplified by a factor of ca. 20. Since BODIPY motifs are not characterized by a unique photophysical signature, alternative chromophores, preferentially without ISC deactivation, should also transform into fluorescent counterparts if an ethylene bridge is installed with appropriate regioselectivity. Building upon the high amplifications detected already at the dimeric state, we believe that an EIE mechanism might also evolve in case of an *intermolecular* encounter of designated, yet identical dye scaffolds. If so, this concept holds promise to refrain from the common *donor–acceptor* setup and serve as a simplified tool for detection and visualization of spatial, molecular recognition processes, similar to the FRET assay, but with modified, functional parameters.

We finally hope that this work can help to further elaborate the paradigms of fluorescence enhancement and support future endeavours in the prosperous field of AIE.

Acknowledgements

L.J.P. acknowledges the Alexander von Humboldt Foundation for his Feodor Lynen postdoctoral fellowship. B.L.F. acknowledges The Ministry of Education, Culture and Science of The Netherlands (Gravitation Program No. 024.001.035 to B.L.F.) and the Horizon 2020 Framework Program (ERC Advanced Investigator Grant No. 694345 to B.L.F.).

Conflict of Interest

The authors declare no conflict of interest.

Data Availability Statement

The data that support the findings of this study are available in the supplementary material of this article.

Keywords: Aggregation-Induced Emission · BODIPY · Dyes · Exciton · Fluorescence

[1] E. E. Jelley, *Nature* **1936**, *138*, 1009–1010.
[2] G. Scheibe, *Angew. Chem.* **1937**, *50*, 212–219.
[3] P. B. Walczak, A. Eisfeld, J. S. Briggs, *J. Chem. Phys.* **2008**, *128*, 044505.
[4] N. J. Hestand, F. C. Spano, *Chem. Rev.* **2018**, *118*, 7069–7163.
[5] F. C. Spano, *Acc. Chem. Res.* **2010**, *43*, 429–439.
[6] S. Choi, J. Bouffard, Y. Kim, *Chem. Sci.* **2014**, *5*, 751–755.
[7] A. C. Benniston, G. Copley, A. Harriman, D. Howgego, R. W. Harrington, W. Clegg, *J. Org. Chem.* **2010**, *75*, 2018–2027.
[8] F. Würthner, T. E. Kaiser, C. R. Saha-Möller, *Angew. Chem. Int. Ed.* **2011**, *50*, 3376–3410; *Angew. Chem.* **2011**, *123*, 3436–3473.
[9] A. S. Davydov, *Sov. Phys. Usp.* **1964**, *7*, 145–178.
[10] J. Frenkel, *Phys. Rev.* **1931**, *37*, 17–44.
[11] J. Frenkel, *Phys. Rev.* **1931**, *37*, 1276–1294.
[12] G. D. Scholes, G. R. Fleming, A. Olaya-Castro, R. van Grondelle, *Nat. Chem.* **2011**, *3*, 763–774.
[13] H. Lee, Y.-C. Cheng, G. R. Fleming, *Science* **2007**, *316*, 1462–1465.
[14] F. Fassioli, R. Dinshaw, P. C. Arpin, G. D. Scholes, *J. R. Soc. Interface* **2014**, *11*, 20130901.
[15] A. Cravcenco, Y. Yu, F. Edhborg, J. F. Goebel, Z. Takacs, Y. Yang, B. Albinsson, K. Börjesson, *J. Am. Chem. Soc.* **2021**, *143*, 19232–19239.
[16] a) A. Schulz, F. Würthner, *Angew. Chem. Int. Ed.* **2022**, *61*, e202114667; *Angew. Chem.* **2022**, *134*, e202114667; b) M. Hecht, P. Leowanawat, T. Gerlach, V. Stepanenko, M. Stolte, M. Lehmann, F. Würthner, *Angew. Chem. Int. Ed.* **2020**, *59*, 17084–17090; *Angew. Chem.* **2020**, *132*, 17232–17238; c) W.

Wagner, M. Wehner, V. Stepanenko, S. Ogi, F. Würthner, *Angew. Chem. Int. Ed.* **2017**, *56*, 16008–16012; *Angew. Chem.* **2017**, *129*, 16224–16228.
[17] H. Marciniak, N. Auerhammer, S. Ricker, A. Schmiedel, M. Holzapfel, C. Lambert, *J. Phys. Chem. C* **2019**, *123*, 3426–3432.
[18] L. J. Patalag, L. P. Ho, P. G. Jones, D. B. Werz, *J. Am. Chem. Soc.* **2017**, *139*, 15104–15113.
[19] A. Bozdemir, H. H. T. Al-Sharif, W. McFarlane, P. G. Waddell, A. C. Benniston, A. Harriman, *Chem. Eur. J.* **2019**, *25*, 15634–15645.
[20] A. B. Nepomnyashchii, A. J. Bard, *Acc. Chem. Res.* **2012**, *45*, 1844–1853.
[21] S. F. Völker, C. Lambert, *Chem. Mater.* **2012**, *24*, 2541–2553.
[22] H. Ceymann, A. Rosspeintner, M. H. Schreck, C. Mützel, A. Stoy, E. Vauthey, C. Lambert, *Phys. Chem. Chem. Phys.* **2016**, *18*, 16404–16413.
[23] R. Liu, G. Zhu, Y. Ji, G. Zhang, *Eur. J. Org. Chem.* **2019**, 3217–3223.
[24] N. Aratani, A. Osuka, Y. H. Kim, D. H. Jeong, D. Kim, *Angew. Chem. Int. Ed.* **2000**, *39*, 1458–1462; *Angew. Chem.* **2000**, *112*, 1517–1521.
[25] Y. H. Kim, D. H. Jeong, D. Kim, S. C. Jeoung, H. S. Cho, S. K. Kim, N. Aratani, A. Osuka, *J. Am. Chem. Soc.* **2001**, *123*, 76–86.
[26] V. S. Lin, S. G. DiMagno, M. J. Therien, *Science* **1994**, *264*, 1105–1111.
[27] N. Auerhammer, A. Schmiedel, M. Holzapfel, C. Lambert, *J. Phys. Chem. C* **2018**, *122*, 11720–11729.
[28] E. Michail, M. H. Schreck, M. Holzapfel, C. Lambert, *Phys. Chem. Chem. Phys.* **2020**, *22*, 18340–18350.
[29] H. Shimizu, K. Fujimoto, M. Furusyo, H. Maeda, Y. Nanai, K. Mizuno, M. Inouye, *J. Org. Chem.* **2007**, *72*, 1530–1533.
[30] J. Ahrens, B. Haberlag, A. Scheja, M. Tamm, M. Bröring, *Chem. Eur. J.* **2014**, *20*, 2901–2912.
[31] C. Lambert, T. Scherpf, H. Ceymann, A. Schmiedel, M. Holzapfel, *J. Am. Chem. Soc.* **2015**, *137*, 3547–3557.
[32] C. Lambert, F. Koch, S. F. Völker, A. Schmiedel, M. Holzapfel, A. Humeniuk, M. I. S. Röhr, R. Mitrić, T. Brixner, *J. Am. Chem. Soc.* **2015**, *137*, 7851–7861.
[33] X. Qiu, R. Lu, H. Zhou, X. Zhang, T. Xu, X. Liu, Y. Zhao, *Tetrahedron Lett.* **2007**, *48*, 7582–7585.
[34] R. Englman, J. Jortner, *Mol. Phys.* **1970**, *18*, 145–164.
[35] M. Kasha, *Radiat. Res.* **1963**, *20*, 55–71.
[36] M. Kasha, R. Rawls, M. A. El-Bayoumi, *Pure Appl. Chem.* **1965**, *11*, 371–392.
[37] E. G. McRae, M. Kasha, *The Molecular Exciton Model in Physical Processes in Radiation Biology* (Eds.: L. Augstein, R. Mason, B. Rosenberg), Academic Press, New York, **1964**, pp. 23–42.
[38] S. Rihn, M. Erdem, A. De Nicola, P. Retailleau, R. Ziessel, *Org. Lett.* **2011**, *13*, 1916–1919.
[39] Y. Hayashi, S. Yamaguchi, W. Y. Cha, D. Kim, H. Shinokubo, *Org. Lett.* **2011**, *13*, 2992–2995.
[40] M. Bröring, R. Krüger, S. Link, C. Kleeberg, S. Köhler, X. Xie, B. Ventura, L. Flamigni, *Chem. Eur. J.* **2008**, *14*, 2976–2983.
[41] B. Ventura, G. Marconi, M. Bröring, R. Krüger, L. Flamigni, *New J. Chem.* **2009**, *33*, 428–438.
[42] J. Ahrens, B. Böker, K. Brandhorst, M. Funk, M. Bröring, *Chem. Eur. J.* **2013**, *19*, 11382–11395.
[43] H. Yokoi, S. Hiroto, H. Shinokubo, *Org. Lett.* **2014**, *16*, 3004–3007.
[44] S. Cherumukkil, S. Ghosh, V. K. Praveen, A. Ajayaghosh, *Chem. Sci.* **2017**, *8*, 5644–5649.
[45] J. Hoche, A. Schulz, L. M. Dietrich, A. Humeniuk, M. Stolte, D. Schmidt, T. Brixner, F. Würthner, R. Mitrić, *Chem. Sci.* **2019**, *10*, 11013–11022.
[46] J. Knoester, *Int. J. Photoenergy* **2006**, 61364.
[47] A. Humeniuk, R. Mitrić, V. Bonačić-Koutecký, *J. Phys. Chem. A* **2020**, *124*, 10143–10151.
[48] H. Fidder, J. Knoester, D. A. Wiersma, *Chem. Phys. Lett.* **1990**, *171*, 529–536.
[49] M. I. S. Röhr, H. Marciniak, J. Hoche, M. H. Schreck, H. Ceymann, R. Mitrić, C. Lambert, *J. Phys. Chem. C* **2018**, *122*, 8082–8093.
[50] B. Scharf, U. Dinur, *Chem. Phys. Lett.* **1984**, *105*, 78–82.
[51] Y.-C. Wei, S. F. Wang, Y. Hu, L.-S. Liao, D.-G. Chen , K.-H. Chang, C.-W. Wang, S.-H. Liu, W.-H. Chan, J.-L. Liao, W.-Y. Hung, T.-H. Wang, P.-T. Chen, H.-F. Hsu, Y. Chi , P.-T. Chou , *Nat. Photonics* **2020**, *14*, 570–577.
[52] A. Loudet, K. Burgess, *Chem. Rev.* **2007**, *107*, 4891–4932.
[53] G. Ulrich, R. Ziessel, A. Harriman, *Angew. Chem. Int. Ed.* **2008**, *47*, 1184–1201; *Angew. Chem.* **2008**, *120*, 1202–1219.
[54] R. Ziessel, A. Harriman, *Chem. Commun.* **2011**, *47*, 611–631.
[55] Z. Shi, X. Han, W. Hu, H. Bai, B. Peng, L. Ji, Q. Fan, L. Li, W. Huang, *Chem. Soc. Rev.* **2020**, *49*, 7533–7567.
[56] O. Altan Bozdemir, S. Erbas-Cakmak, O. O. Ekiz, A. Dana, E. U. Akkaya, *Angew. Chem. Int. Ed.* **2011**, *50*, 10907–10912; *Angew. Chem.* **2011**, *123*, 11099–11104.
[57] L. J. Patalag, S. Ahadi, O. Lashchuk, P. G. Jones, S. Ebbinghaus, D. B. Werz, *Angew. Chem. Int. Ed.* **2021**, *60*, 8766–8771; *Angew. Chem.* **2021**, *133*, 8848–8853.
[58] A. Patra, L. J. Patalag, P. G. Jones, D. B. Werz, *Angew. Chem. Int. Ed.* **2021**, *60*, 747–752; *Angew. Chem.* **2021**, *133*, 758–763.
[59] K. Sitkowska, M. F. Hoes, M. M. Lerch, L. N. Lameijer, P. van der Meer, W. Szymański, B. L. Feringa, *Chem. Commun.* **2020**, *56*, 5480–5483.
[60] K. Sitkowska, B. L. Feringa, W. Szymanski, *J. Org. Chem.* **2018**, *83*, 1819–1827.
[61] G. Das, S. Cherumukkil, A. Padmakumar, V. B. Banakar, V. K. Praveen, A. Ajayaghosh, *Angew. Chem. Int. Ed.* **2021**, *60*, 7851–7859; *Angew. Chem.* **2021**, *133*, 7930–7938.
[62] Y. Ito, T. Konoike, T. Saegusa, *J. Am. Chem. Soc.* **1975**, *97*, 2912–2914.
[63] M. Blangetti, P. Fleming, D. F. O'Shea, *J. Org. Chem.* **2012**, *77*, 2870–2877.
[64] a) S. Kozuch, D. Guzman, J. L. M. Martin, *J. Phys. Chem. C* **2010**, *114*, 20801–20808; b) S. Grimme, J. Antony, S. Ehrlich, H. Krieg, *J. Chem. Phys.* **2010**, *132*, 154104; c) L. Goerigk, A. Hansen, C. Bauer, S. Ehrlich, A. Najibi, S. Grimme, *Phys. Chem. Chem. Phys.* **2017**, *19*, 32184–32215.
[65] C. Zhong, D. Bialas, C. J. Collison, F. C. Spano, *J. Phys. Chem. C* **2019**, *123*, 18734–18745.
[66] E. Rousseau, M. Van der Auweraer, F. C. De Schryver, *Langmuir* **2000**, *16*, 8865–8870.
[67] A. Turkin, P. Maly, C. Lambert, *Phys. Chem. Chem. Phys.* **2021**, *23*, 18393–18403.
[68] A. Prlj, L. Vannay, C. Corminboeuf, *Helv. Chim. Acta* **2017**, *100*, e1700093.
[69] L. Jiao, C. Yu, J. Wang, E. A. Briggs, N. A. Besley, D. Robinson, M. J. Ruedas-Rama, A. Orte, L. Crovetto, E. M. Talavera, J. M. Alvarez-Pez, M. Van der Auweraer, N. Boens, *RSC Adv.* **2015**, *5*, 89375–89388.
[70] C. Goze, G. Ulrich, L. J. Mallon, B. D. Allen, A. Harriman, R. Ziessel, *J. Am. Chem. Soc.* **2006**, *128*, 10231–10239.
[71] M. Kusinski, J. Nagesh, M. Gladkikh, A. F. Izmaylov, R. A. Jockusch, *Phys. Chem. Chem. Phys.* **2019**, *21*, 5759–5770.
[72] T. Abe, A. Miyazawa, H. Konno, Y. Kawanishi, *Chem. Phys. Lett.* **2010**, *491*, 199–202.

[73] U. Mayerhöffer, B. Fimmel, F. Würthner, *Angew. Chem. Int. Ed.* **2012**, *51*, 164–167; *Angew. Chem.* **2012**, *124*, 168–171.
[74] U. Mayerhöffer, M. Gsänger, M. Stolte, B. Fimmel, F. Würthner, *Chem. Eur. J.* **2013**, *19*, 218–232.
[75] R. Lincoln, L. E. Greene, C. Bain, J. O. Flores-Rizo, D. S. Bohle, G. Cosa, *J. Phys. Chem. B* **2015**, *119*, 4758–4765.
[76] A. Prlj, A. Fabrizio, C. Corminboeuf, *Phys. Chem. Chem. Phys.* **2016**, *18*, 32668–32672.
[77] F. Li, S. I. Yang, Y. Ciringh, J. Seth, C. H. Martin III, D. L. Singh, D. Kim, R. R. Birge, D. F. Bocian, D. Holten, J. S. Lindsey, *J. Am. Chem. Soc.* **1998**, *120*, 10001–10017.
[78] H. L. Kee, C. Kirmaier, L. H. Yu, P. Thamyongkit, W. J. Youngblood, M. E. Calder, L. Ramos, B. C. Noll, D. F. Bocian, W. R. Scheidt, R. R. Birge, J. S. Lindsey, D. Holten, *J. Phys. Chem. B* **2005**, *109*, 20433–20443.
[79] J. A. Levitt, P. H. Chung, M. K. Kuimova, G. Yahioglu, Y. Wang, J. L. Qu, K. Suhling, *ChemPhysChem* **2011**, *12*, 662–672.
[80] Y. Wu, M. Frasconi, W.-G. Liu, R. M. Young, W. A. Goddard III, M. R. Wasielewski, J. F. Stoddart, *J. Am. Chem. Soc.* **2020**, *142*, 11835–11846.
[81] Z. Liu, Z. Jiang, M. Yan, X. Wang, *Front. Chem.* **2019**, *7*, 712.
[82] M. K. Kuimova, G. Yahioglu, J. A. Levitt, K. Suhling, *J. Am. Chem. Soc.* **2008**, *130*, 6672–6673.
[83] I. López-Duarte, T. T. Vu, M. A. Izquierdo, J. A. Bull, M. K. Kuimova, *Chem. Commun.* **2014**, *50*, 5282–5284.
[84] Y. L. Wu, M. Stefl, A. Olzynska, M. Hof, G. Yahioglu, P. Yip, D. R. Casey, O. Ces, J. Humpolickova, M. K. Kuimova, *Phys. Chem. Chem. Phys.* **2013**, *15*, 14986–14993.
[85] T. Suhina, S. Amirjalayer, S. Woutersen, D. Bonnb, A. M. Brouwer, *Phys. Chem. Chem. Phys.* **2017**, *19*, 19998–20007.
[86] a) N. L. C. Leung, N. Xie, W. Yuan, Y. Liu, Q. Wu, Q. Peng, Q. Miao, J. W. Y. Lam, B. Z. Tang, *Chem. Eur. J.* **2014**, *20*, 15349–15353; b) Y. Tu, J. Liu, H. Zhang, Q. Peng, J. W. Y. Lam, B. Z. Tang, *Angew. Chem. Int. Ed.* **2019**, *58*, 14911–14914; *Angew. Chem.* **2019**, *131*, 15053–15056.
[87] a) X.-L. Peng, S. Ruiz-Barragan, Z.-S. Li, Q.-S. Li, L. Blancafort, *J. Mater. Chem. C* **2016**, *4*, 2802–2810; b) R. Crespo-Otero, Q. Li, L. Blancafort, *Chem. Asian J.* **2019**, *14*, 700–714.
[88] a) Z. Zhao, H. Zhang, J. W. Y. Lam, B. Z. Tang, *Angew. Chem. Int. Ed.* **2020**, *59*, 9888–9907; *Angew. Chem.* **2020**, *132*, 9972–9993; b) J. Mei, N. L. C. Leung, R. T. K. Kwok, J. W. J. Lam, B. Z. Tang, *Chem. Rev.* **2015**, *115*, 11718–11940.
[89] K. Kokado, K. Sada, *Angew. Chem. Int. Ed.* **2019**, *58*, 8632–8639; *Angew. Chem.* **2019**, *131*, 8724–8731.
[90] F. Würthner, *Angew. Chem. Int. Ed.* **2020**, *59*, 14192–14196; *Angew. Chem.* **2020**, *132*, 14296–14301.
[91] H. Sunahara, Y. Urano, H. Kojima, T. Nagano, *J. Am. Chem. Soc.* **2007**, *129*, 5597–5604.
[92] W. Qin, M. Baruah, M. Van der Auweraer, F. C. De Schryver, N. Boens, *J. Phys. Chem. A* **2005**, *109*, 7371–7384.
[93] Owing to the rapidly growing amount of (CT)-excited states at the oligomers, a valid quantification of their influences on (non-)radiative decay channels revealed to be too complex and goes beyond the scope of this study.
[94] W. Li, L. Li, H. Xiao, R. Qi, Y. Huang, Z. Xie, X. Jing, H. Zhang, *RSC Adv.* **2013**, *3*, 13417–13421.
[95] J. T. Ly, K. F. Presley, T. M. Cooper, L. A. Baldwin, M. J. Dalton, T. A. Grusenmeyer, *Phys. Chem. Chem. Phys.* **2021**, *23*, 12033–12044.
[96] L. Yang, X. Wang, G. Zhang, X. Chen, G. Zhanga, J. Jiang, *Nanoscale* **2016**, *8*, 17422–17426.
[97] J. G. Woller, J. K. Hannestad, B. Albinsson, *J. Am. Chem. Soc.* **2013**, *135*, 2759–2768.
[98] J.-D. Yi, D.-H. Si, R. Xie, Q. Yin, M.-D. Zhang, Q. Wu, G.-L. Chai, Y.-B. Huang, R. Cao, *Angew. Chem. Int. Ed.* **2021**, *60*, 17108–17114; *Angew. Chem.* **2021**, *133*, 17245–17251.
[99] L. Zhang, G. Ng, N. Kapoor-Kaushik, X. Shi, N. Corrigan, R. Webster, K. Jung, C. Andre, J. M. Boyer, *Angew. Chem. Int. Ed.* **2021**, *60*, 22664–22671; *Angew. Chem.* **2021**, *133*, 22846–22853.
[100] S. Garg, H. Schwartz, M. Kozlowska, A. B. Kanj, K. Müller, W. Wenzel, U. Ruschewitz, L. Heinke, *Angew. Chem. Int. Ed.* **2019**, *58*, 1193–1197; *Angew. Chem.* **2019**, *131*, 1205–1210.
[101] K. Trofymchuk, A. Reisch, P. Didier, F. Fras, P. Gilliot, Y. Mely, A. S. Klymchenko, *Nat. Photonics* **2017**, *11*, 657–663.
[102] G. P. Acuna, F. M. Möller, P. Holzmeister, S. Beater, B. Lalkens, P. Tinnefeld, *Science* **2012**, *338*, 506–510.

Manuscript received: December 9, 2021
Accepted manuscript online: March 4, 2022
Version of record online: March 16, 2022